

Anomalous anisotropy of spin current in a cubic spin source with noncollinear antiferromagnetism

Cuimei Cao^{1a}, Shiwei Chen^{2,6a}, Rui-Chun Xiao³, Zengtai Zhu^{4,5}, Guoqiang Yu^{4,5},
Yangping Wang¹, Xuepeng Qiu⁶, Liang Liu⁷, Tieyang Zhao⁷, Ding-Fu Shao^{8,*}, Yang
Xu^{1,*}, Jingsheng Chen^{7,*}, and Qingfeng Zhan^{1,*}

¹*Key Laboratory of Polar Materials and Devices (MOE), School of Physics and Electronic
Science, East China Normal University, Shanghai 200241, People's Republic of China*

²*Faculty of Physics and Electronic Science, Hubei University, Wuhan 430062, People's
Republic of China*

³*Institute of Physical Science and Information Technology, Anhui University, Hefei 230601,
China*

⁴*Songshan Lake Materials Laboratory, Dongguan, Guangdong 523808, People's Republic of
China*

⁵*Beijing National Laboratory for Condensed Matter, Physics Institute of Physics, Chinese
Academy of Sciences, Beijing 100190, People's Republic of China*

⁶*Shanghai Key Laboratory of Special Artificial Microstructure Materials, School of Physics
Science and Engineering, Tongji University, Shanghai 200092, People's Republic of China*

⁷*Department of Materials Science and Engineering, National University of Singapore,
Singapore, Singapore.*

⁸*Key Laboratory of Materials Physics, Institute of Solid State Physics, HFIPS, Chinese
Academy of Sciences, Hefei 230031, China*

^{a)} C. Cao and S. Chen contributed equally to this work.

* Authors to whom correspondence should be addressed: dfshao@issp.ac.cn,
yxu@phy.ecnu.edu.cn, msecj@nus.edu.sg, qfzhan@phy.ecnu.edu.cn

**Cubic materials host high crystal symmetry and hence are not expected to support
anisotropy in transport phenomena. In contrast to this common expectation, here**

we report an anomalous anisotropy of spin current can emerge in the (001) film of Mn₃Pt, a noncollinear antiferromagnetic spin source with face-centered cubic structure. Such spin current anisotropy originates from the intertwined time reversal-odd (\mathcal{T} -odd) and time reversal-even (\mathcal{T} -even) spin Hall effects. Based on symmetry analyses and experimental characterizations of the current-induced spin torques in Mn₃Pt-based heterostructures, we find that the spin current generated by Mn₃Pt (001) exhibits exotic dependences on the current direction for all the spin components, deviating from that in conventional cubic systems. We also demonstrate that such an anisotropic spin current can be used to realize low-power spintronic applications such as the efficient field-free switching of the perpendicular magnetizations.

The anisotropy of transport phenomena is determined by the group symmetry and hence emerges in materials with low symmetry¹⁻³. The high-symmetry cubic materials widely used in electronic devices are usually not expected to host a strong transport anisotropy. A typical example is the widely used cubic structured spin source materials such as Pt, which hosts the isotropic spin Hall effect (SHE) to generate an out-of-plane spin current and the associated spin-orbit torque (SOT) for the manipulation of the magnetizations in spintronic devices⁴. The performance of such a device is independent of the current direction since the spin Hall conductivity (SHC) σ_{zx}^y (in the form of σ_{ij}^p , where i, j , and p are the generated spin-current, the driven charge-current, and spin polarization directions, respectively) is invariant under rotation transformations of the coordinate system^{5,6}. It would be interesting from the fundamental point of view and desirable for spintronic applications to find a new mechanism for the emergence of the anisotropic spin current in cubic spin sources even with the high symmetry film directions.

Here we demonstrate that an anomalous anisotropy of the spin current can be generated in noncollinear antiferromagnetic Mn₃X (X = Pt, Ir, or Rh) family with face-centered cubic structure even for the high symmetric (001) film, due to the noncollinear antiferromagnetism and hence the intertwined time-reversal-even (\mathcal{T} -even) and time-

reversal-odd (\mathcal{T} -odd) parts of SHE. The noncollinear magnetic configuration of Mn_3X allows not only conventional SHC σ_{zx}^y but also unconventional σ_{zx}^x , σ_{zx}^z , and all of them exhibit exotic dependence on the current direction. Using Mn_3Pt as a representative example, we confirm the anisotropic σ_{zx}^p by the measurements of the current-induced spin-torque ferromagnetic resonance (ST-FMR) and the anomalous Hall effect (AHE) loop shift of the ferromagnetic layers adjacent to the Mn_3Pt layer in a SOT device. We also show this spin current can realize efficient field-free switching of the perpendicular magnetizations in ferromagnets, and the switching performances can be optimized according to such an anomalous anisotropy.

Mn_3X ($\text{X} = \text{Pt}, \text{Ir}$ or Rh) is a material family that crystallizes in a cubic Cu_3Au -type structure^{7,8}. As depicted in Fig. 1, the Mn atoms form kagome-type lattice planes stacked along the $[111]$ direction. In its paramagnetic phase at high temperatures (Fig. 1a), the preserved time-reversal symmetry (\mathcal{T}) only allows the \mathcal{T} -even SHE^{9,10}, and the space group $Pm\bar{3}m$ enforces the isotropic $\sigma_{zx}^{y,\text{even}}$, i.e. $\sigma_{zx}^{y,\text{even}}(\phi_E = 0^\circ) = \sigma_{zx}^{y,\text{even}}(\phi_E \neq 0^\circ)$, where ϕ_E is used to denote the in-plane current direction with respect to an in-plane reference direction $[100]$. In an SOT device where a ferromagnetic layer with a perpendicular magnetization is deposited on the Mn_3X (001) film (Fig. 1b), an out-of-plane y -polarized spin current independent of the in-plane charge current direction can be generated in Mn_3X , which enters the top ferromagnetic layer and exert a damping-like torque $\sim \mathbf{m} \times (\mathbf{m} \times \mathbf{y})$ to switch the ferromagnetic magnetization⁹. Such a switching requires a high current density and an external assisting magnetic field for deterministic switching and hence is inefficient for realistic applications.

Below the Néel temperature (T_N), Mn_3X is antiferromagnetic with a noncollinear “head-to-head” or “tail-to-tail” alignments of Mn moments in the kagome planes (Fig. 1c). Its magnetic space group $R\bar{3}m'$ allows not only the conventional $\sigma_{zx}^{y,\text{even}}$ but also the unconventional $\sigma_{zx}^{x,\text{even}}$ and $\sigma_{zx}^{z,\text{even}}$. The magnitudes of the \mathcal{T} -even SHC are the same for currents along the primary directions $[100]$ ($\phi_E = 0^\circ$) and $[010]$ ($\phi_E = 90^\circ$) (Supplementary Note 1). On the other hand, the noncollinear antiferromagnetism breaks the \mathcal{T} symmetry and introduces non-spin-degenerate Fermi surfaces in Mn_3X ,

which contribute to the \mathcal{T} -odd SHE (also termed as magnetic SHE, MSHE)¹¹ with the SHC that also have the same magnitudes for currents along the primary directions [100] ($\phi_E = 0^\circ$) and [010] ($\phi_E = 90^\circ$) (Supplementary Note 1). However, the net SHC contributed by the intertwined \mathcal{T} -even and \mathcal{T} -odd SHE has a more complicated anisotropy:

$$\begin{aligned}\sigma_{zx}^x(\phi_E) &\propto \lambda_x \cos 2\phi_E + \mu_x \sin 2\phi_E, \\ \sigma_{zx}^y(\phi_E) &\propto \lambda_y \sin 2\phi_E + \mu_y \cos 2\phi_E, \\ \sigma_{zx}^z(\phi_E) &\propto \lambda_z \cos \phi_E + \mu_z \sin \phi_E,\end{aligned}\tag{1}$$

where λ_i and μ_i are constants and can be used to estimate the relative strength of \mathcal{T} -even and \mathcal{T} -odd SHE. Figure 1e schematically show the ϕ_E dependence of σ_{zx}^p and its decomposition into the \mathcal{T} -even and \mathcal{T} -odd components using arbitrary parameters (see discussion in Supplementary Note 1). Such anisotropy is anomalous for cubic systems, and particularly unexpected for the high symmetric (001) plane. Figure 1d illustrates the SOT exerted by the anisotropic spin current in Mn_3X . The existence of an unconventional torque component $\sim \mathbf{m} \times (\mathbf{m} \times \mathbf{z})$ can directly change the effective damping and allows the efficient field-free switching of perpendicular magnetization with a small current¹². One can further design the in-plane current direction for a maximum z-polarization in the out-of-plane spin current to optimize the performance of the SOT device.

Here, we use Mn_3Pt to demonstrate the anomalous anisotropy of spin current in Mn_3X , which has a T_N of ~ 475 K^{7,8,13,14}. We first investigate the current-induced SOT in (001)-oriented Mn_3Pt /permalloy (Py) heterostructures by the ST-FMR technique. More details about the sample preparation and characterization are provided in Methods and Supplementary Note 2. The Mn_3Pt /Py heterostructure is patterned with microwave-compatible contacts whose orientation is varied to study the SOT anisotropy as a function of the azimuthal angle ϕ_E , i.e., the angle between the microwave current I_{rf} and the [100] direction of Mn_3Pt , as illustrated in Fig. 2a. Here the x, y, z axes form local frames that change with the direction of I_{rf} , i.e., I_{rf} is always along x . For each device with a fixed ϕ_E , an in-plane external magnetic field $H_{\text{ext}}^{\parallel}$ is swept at an angle

ϕ_H with respect to I_{rf} (Fig. 2a). The ST-FMR signal is a rectified voltage V_{mix} , whose lineshape can be decomposed into a symmetric component V_s and an antisymmetric component V_a near the resonant condition¹⁵, characterizing the in-plane SOT τ_{\parallel} and out-of-plane SOT τ_{\perp} , respectively, allowing the full determination of the damping-like and field-like SOT from all possible spin polarizations (Supplementary Note 3)^{16,17}. For the in-plane \mathbf{m} of Py, τ_{\perp} may come from the damping-like SOT associated with σ_{zx}^z , while it also includes the field-like contribution from σ_{zx}^y , σ_{zx}^x , and the Oersted field.

In our Pt/Py reference sample, V_{mix} is centrosymmetric about $H_{\text{ext}}^{\parallel}$, since the spin current is generated solely from the conventional SHE and Oersted field (Supplementary Note 3). In Mn₃Pt, however, the measured V_{mix} ($\phi_H = 10^\circ$) does not overlap with $-V_{\text{mix}}$ ($\phi_H = 190^\circ$), i.e., V_{mix} does not exhibit a perfect inversion with the reversal of $H_{\text{ext}}^{\parallel}$, indicating the presence of unconventional SOT associated with the SHC other than σ_{zx}^y (Supplementary Note 3)^{1,18-23}.

For further investigation, we measure the ϕ_H dependence of V_a and V_s at various ϕ_E (Supplementary Note 4). The ϕ_H dependence can be fitted by^{1,15,19,24}:

$$V_a = A_{\text{FL}}^y \cos \phi_H \sin 2\phi_H + A_{\text{FL}}^x \sin \phi_H \sin 2\phi_H + A_{\text{DL}}^z \sin 2\phi_H, \quad (2)$$

$$V_s = S_{\text{DL}}^y \cos \phi_H \sin 2\phi_H + S_{\text{DL}}^x \sin \phi_H \sin 2\phi_H + S_{\text{FL}}^z \sin 2\phi_H, \quad (3)$$

where S_{DL}^y , S_{DL}^x , and A_{DL}^z are coefficients for the damping-like SOT associated with σ_{zx}^y , σ_{zx}^x , and σ_{zx}^z , respectively, while A_{FL}^y , A_{FL}^x , and S_{FL}^z correspond to the field-like counterparts. Note that the contribution of the field-like SOT from the Oersted field is included in A_{FL}^y . We show in Fig. 2b how V_s ($\phi_E = 45^\circ$) is decomposed into the contributions from σ_{zx}^p (see Supplementary Note 4 for V_a and V_s at $\phi_E = 0^\circ, 45^\circ$, and 90°). Important observations can be made: (i) Despite a subdominant contribution, the presence of nonzero σ_{zx}^x and σ_{zx}^z is evident, consistent with the asymmetric V_{mix} ($H_{\text{ext}}^{\parallel}$) mentioned above. (ii) Compared to the case of $\phi_E = 0^\circ$, the σ_{zx}^z contribution is enhanced for $\phi_E = 45^\circ$ (Supplementary Note 4), consistent with the previous observation of a stronger (weaker) σ_{zx}^z for I_{rf} applied parallel (perpendicular) to the

magnetic mirror plane of Mn₃Pt²¹. (iii) A notable discrepancy can be seen between the cases of $\phi_E = 0^\circ$ and $\phi_E = 90^\circ$, which is unexpected considering their equivalency in both the crystal and magnetic structures. This is different to previous reports in cubic systems where the anisotropic spin currents have never been observed in (001) films with the highest crystal symmetry^{20,25}.

To better visualize the SOT anisotropy, we show in Figs. 2c-2e the ϕ_E dependence of the damping-like SOT efficiency per unit current density $\xi_{DL,j}^P$ (see Supplementary Note 5 for more details)^{15,22}. In principle, one can derive the relative magnitudes of σ_{zx}^y , σ_{zx}^x , and σ_{zx}^z by fitting the ϕ_E dependence of $\xi_{DL,j}^P$ using Eq. (1). The fitted nonzero values of $\lambda_y = 0.04359$, $\mu_y = 0.01126$, $\lambda_x = 0.00328$, $\mu_x = 0.02038$, $\lambda_z = 0.02049$, and $\mu_z = 0.03176$ qualitatively indicate the intertwined \mathcal{T} -even and \mathcal{T} -odd SHE, which results in a discrepancy between the signal at $\xi_{DL,j}^i$ ($\phi_E = 0^\circ$) and $\xi_{DL,j}^i$ ($\phi_E = 90^\circ$).

Since the unconventional z -polarized spin current is important for low-power switching of high-density spintronic devices with perpendicular magnetizations, we build Mn₃Pt(5)/Ti(3)/CoFeB(1)/MgO(2)/SiO₂(2) heterostructures (numbers in parentheses indicate layer thickness in nanometers) with perpendicular magnetic anisotropy (PMA) to further quantify σ_{zx}^z (Fig. 3a). The PMA of this heterostructure is confirmed by the square hysteresis loop in the Hall resistance R_{xy} as a function of the out-of-plane magnetic field H_{ext}^z (Supplementary Note 6).

We first perform the AHE loop shift measurement on the PMA heterostructures²⁶. As shown in Fig. 3b, the AHE loop under an out-of-plane magnetic field H_{ext}^z and $I = 1$ mA along [110] (i.e., $\phi_E = 45^\circ$) almost overlaps with the loop under $I = -1$ mA. However, as shown in Fig. 3c, when I is increased to ± 16 mA, considerable AHE loop shift occurs, i.e., the center of the loop is shifted to positive (negative) field values for positive (negative) I . Such a shift is indicative of an effective field H_{eff}^z acting in conjunction with the external H_{ext}^z (see also Supplementary Note 7 and Note 8). Figure 3d depicts the I dependence of H_{eff}^z (see Methods) for selected ϕ_E of 0° , 45° , and 90° . Echoing the qualitatively different behavior between $I = \pm 1$ and ± 16 mA, a clear threshold current effect is evident: H_{eff}^z abruptly increases from near zero when I is

greater than a threshold value²⁶, characteristic of a damping-like τ_{\perp} originating from σ_{zx}^z ^{3,12,26,27}.

To better visualize the anisotropy of H_{eff}^z which characterizes the anisotropy of σ_{zx}^z and the associated τ_{\perp} , we plot in Fig. 3e the ϕ_E dependence of the H_{eff}^z/J , where J is the applied in-plane current density. With increasing ϕ_E , H_{eff}^z/J first increases to a maximum for $\phi_E = 45^\circ$, and then decreases and changes the sign around $\phi_E = 135^\circ$. The H_{eff}^z/J for $\phi_E = 0^\circ$ is about a half of that for $\phi_E = 90^\circ$. This behavior is consistent with the ϕ_E dependence of $\xi_{\text{DL},j}^z$ measured by ST-FMR (Fig. 2e). Therefore, based on the similar results from two different measurements, we confirm the anomalous anisotropy of the spin current in Mn₃Pt which is not expected by the cubic crystal symmetry. The ϕ_E dependence of H_{eff}^z/J can be well fitted using Eq. (1) (Fig. 3e), yielding parameters $\lambda_z = 3.48$ and $\mu_z = 9.59$. $\lambda_z/\mu_z = 0.36$ indicates that such an anomalous anisotropy is originated from the coexistence of \mathcal{T} -odd and \mathcal{T} -even SHE in Mn₃Pt, where \mathcal{T} -odd SHE is predominating.

The existence of σ_{zx}^z allows the field-free deterministic switching of the perpendicular magnetization in the CoFeB layer adjacent to Mn₃Pt. As shown in Fig. 4a, the injected pulse current, when above a threshold value, is able to change the sign of R_{xy} for various ϕ_E , indicating that deterministic magnetization switching of the PMA CoFeB layer has been realized without an in-plane assistant field (see Methods and Supplementary Note 9 for more details). The change of the switching Hall resistance is represented by ΔR_{xy} , which is the half of the difference between R_{xy} at zero current after the application of the positive and negative current pulses. We find that the ϕ_E dependence of ΔR_{xy} is consistent with that of H_{eff}^z/J (Fig. 4b). The largest ΔR_{xy} corresponding to a switching ratio of $\approx 77\%$ is achieved when H_{eff}^z/J is maximum around $\phi_E = 45^\circ$, indicating the optimal current direction for designing SOT devices based on Mn₃Pt.

The magnetic space group $R\bar{3}m'$ supports a small but nonvanishing net magnetization in Mn₃Pt. The presence of such a net magnetization allows the switching of the magnetic order parameter by a small magnetic field, which is equivalent to the

\mathcal{T} -operation which changes the sign of the \mathcal{T} -odd SHC but does not influence the \mathcal{T} -even SHC^{12,28}. This property can be used to verify whether \mathcal{T} -odd SHE dominates the anisotropic spin current in Mn₃Pt and hence the field-free switching of the perpendicular magnetization. Here we perform the current-induced magnetization switching measurements for $\phi_E = 0^\circ$ with the application of a premagnetization field H_{pre} of 8 T along the [001] direction, which aligns the magnetic order parameter of Mn₃Pt as depicted in the inset of Fig. 4c. The polarity of the field-free switching is anticlockwise in this case (Fig. 4d). Applying the H_{pre} to the [00 $\bar{1}$] direction reverses the magnetic order parameter of Mn₃Pt and changes the switching polarity to clockwise. This clearly proves the predominating role of the \mathcal{T} -odd SHE²⁹ for the spin current in Mn₃Pt and hence the field-free switching of the perpendicular magnetization.

In summary, we observed an unexpected anisotropy of spin current in Mn₃Pt, a cubic structured spin source with noncollinear antiferromagnetism due to the intertwined \mathcal{T} -odd and \mathcal{T} -even SHE. We also show the spin current generated in Mn₃Pt can be used to realize efficient field-free SOT switching of ferromagnets PMA and the anomalous anisotropy can be used to optimize the switching performance. Our work offers a new route to introduce transport anisotropy in materials with high crystal symmetry, which is beneficial for designing and engineering of low-power and high-performance electronic devices.

Methods

Sample preparation. Samples of Mn₃Pt, Mn₃Pt/Ti/CoFeB/MgO/SiO₂, Mn₃Pt/Py and Pt/Py bilayers were deposited on MgO(001) substrates by DC/RF magnetron sputtering with a base pressure of 1×10^{-7} Torr. Note that the metallic and oxide films were deposited by using DC and RF magnetron sputtering, respectively. For the deposition of Mn₃Pt, the MgO(001) substrate was pre-annealed for 1 h at 700 °C before deposition to obtain a smooth and clean substrate. The deposition was performed at 500 °C. The Ar gas pressure and sputtering power were 2 mTorr and 40 W, respectively. After deposition, the Mn₃Pt film was heated to 550 °C for 1.5 h to improve the crystalline quality. After cooling down to room temperature, the Ti/CoFeB/MgO/SiO₂ multilayer or the Py layer were deposited onto the Mn₃Pt film, respectively. The Mn₃Pt/Ti/CoFeB/MgO/SiO₂ heterostructure was *in situ* annealed at 200 °C for 30 min under vacuum conditions to promote PMA. In this structure, the nonmagnetic interlayer Ti was used to provide the PMA of CoFeB and magnetically decouple the Mn₃Pt and CoFeB layers²⁷, and hence it does not contribute to the magnetization switching (Supplementary Note 10). The SOT contribution from the Ti layer is negligible due to the extremely small spin Hall angle of Ti^{27,30}. A 2 nm SiO₂ capping layer was used to protect its underlayers. For the Mn₃Pt(12 nm)/Py (Ni₈₀Fe₂₀, 13 nm) bilayer used in the ST-FMR measurements, the Py film was prepared at room temperature, with the Ar gas pressure and sputtering power being 2 mTorr and 40 W, respectively. The control sample Pt/Py bilayers used for the ST-FMR measurements were deposited at room temperature and the Ar gas pressure and sputtering power for the Pt film were 2 mTorr and 20 W, respectively. The film thicknesses were controlled by the deposition time with a pre-calibrated deposition rate as determined by X-ray reflectivity measurements.

Device fabrication. In order to investigate the anisotropy of the spin-orbit torque of cubic Mn₃Pt, samples of Mn₃Pt/Ti/CoFeB/MgO and Mn₃Pt (Pt)/Py were patterned into Hall bars (10 μm × 50 μm) and microstrip devices (20 μm × 50 μm), respectively, using a combination of photolithography and ion beam etching. Then, a top electrode of Ti(5 nm)/Cu(100 nm) was deposited by DC magnetron sputtering. For devices with different

current directions in the sample plane, ϕ_E ranges from 0° to 180° with a step of 15° .

Sample characterization. The thickness and crystal structure were characterized by X-ray reflectivity and high-resolution X-ray diffraction techniques with a Bruker D8 Discover diffractometer using Cu K_α radiation ($\lambda = 0.15419$ nm). The magnetic and electrical properties were measured in a magnetic property measurement system (MPMS, Quantum Design) and physical property measurement system (PPMS, Quantum Design), respectively.

ST-FMR measurements. The ST-FMR signals (V_{mix}) were measured by a Stanford Research SR830 lock-in amplifier. In the angular-dependent ST-FMR measurements, the applied microwave current with frequency and nominal power were 7 GHz and 18 dBm, respectively.

AHE loop shift measurements. The existence of H_{eff}^Z was verified by the AHE loop shift measurements with different pulse currents, where H_{eff}^Z is defined as the shift of the loop $H_{\text{eff}}^Z(I) = [|H_{\text{rev}}^+(I)| - |H_{\text{rev}}^-(I)|] / 2$, with $H_{\text{rev}}^\pm(I)$ being the positive and negative magnetization-reversal fields.

Current-induced magnetization switching measurements. The current-induced magnetization measurements were conducted by utilizing a Keithley 6221 current source and a 2182 nano voltmeter. For each experimental data point in the R_{xy} - I loop, a pulse d.c. current I_p with a duration of 200 μs was applied to the Hall bar device as the write current. Then, a small probe pulse current of 0.1 mA with a duration of 2 ms was applied to monitor the R_{xy} . The amplitude of the write pulse current was varied to obtain a complete R_{xy} - I loop.

Data availability

The data that support the findings of this study are available from the corresponding authors upon reasonable request.

Acknowledgements

This work was supported by the National Natural Science Foundation of China (Grant Nos. 12174103, 12274411 and 12274125), the Natural Science Foundation of Shanghai (Grant Nos. 21ZR1420500 and 21JC1402300), the Shanghai Pujiang Program (Grant No. 21PJ1403100) and Natural Science Foundation of Anhui Province (Grant No. 2208085QA08).

Author contributions

C.C. and S.C. conceived the idea and designed the experiment, D.F.S., Y.X., J.C. and Q.Z. supervised the project. C.C. and Y.W. grew the samples and performed the structural characterizations. S.C. fabricated the devices. C.C. and S.C. performed electrical transport measurements and analyzed the results together with X.Q. Z.Z. and G.Y. performed the ST-FMR measurements. L.L., T.Z. and J.C. gave suggestions on the experiments. R.C.X. and D.F.S. performed the theoretical analyses. All authors contributed to discussions. C.C., S.C., D.F.S. and Y.X. wrote the manuscript with input from all authors.

Competing interests

The authors declare no competing interests.

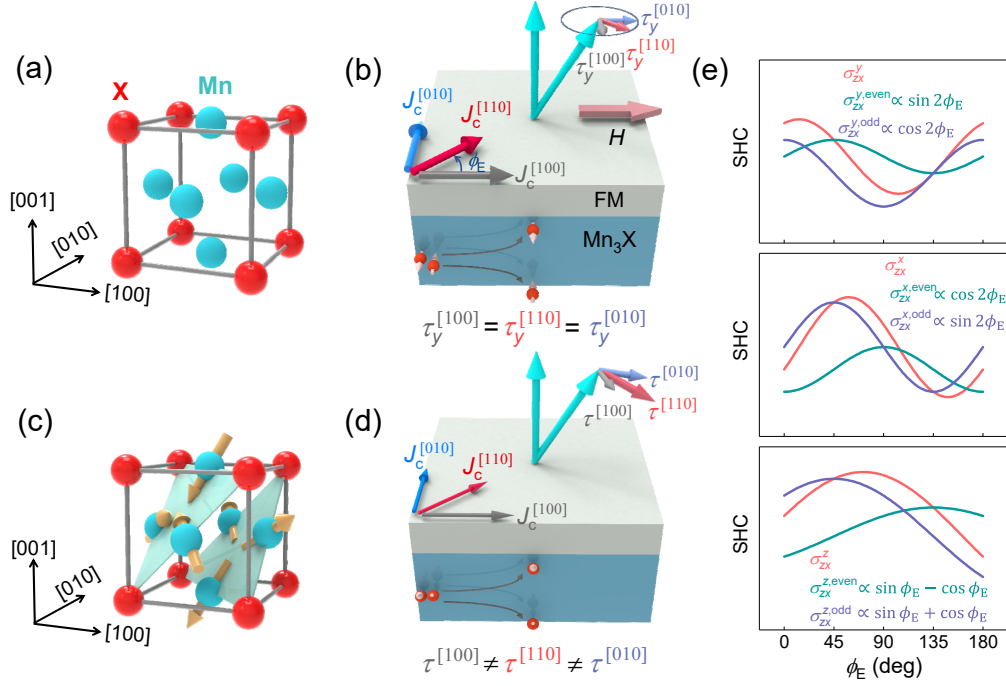


Fig. 1 Anisotropy of the spin current polarization and the associated SOT in spin source materials with a cubic structure. **a** The crystal structure of cubic Mn_3X ($X= Pt, Ir$ or Rh) in paramagnetic state. **b**, A schematic of a SOT device using paramagnetic Mn_3X as the spin source, where an isotropic and y -polarized spin current generated in the bottom Mn_3X layer enters the adjacent ferromagnetic (FM) layer, exert an isotropic SOT $\sim \mathbf{m} \times (\mathbf{m} \times \mathbf{y})$ on the perpendicular magnetization. ϕ_E is the angle between the current and the $[100]$ direction of Mn_3X . In this case, a sizable external magnetic field is required for a deterministic switching, and the charge current required is large. **c**, The structure of cubic Mn_3X with noncollinear antiferromagnetism, where the Mn moments form “head-to-head” or “tail-to-tail” noncollinear alignments in (111) kagome planes. **d**, A schematic of a SOT device using noncollinear antiferromagnetic Mn_3X as the spin source, where an anisotropic spin current generated by Mn_3X exerts the anisotropic SOT in the adjacent ferromagnetic layer. The presence of the z -polarization in the spin current and the associated unconventional SOC component $\sim \mathbf{m} \times (\mathbf{m} \times \mathbf{z})$ allows a field-free switching of perpendicular magnetization, which does not require a large charge current. **e**, Theoretical ϕ_E dependence of the SHC σ_{zx}^p ($p = y, x, z$) and its decomposition into the contributions from the \mathcal{T} -even and \mathcal{T} -odd SHE in Mn_3X . The parameters used to plot (e) are shown in Supplementary Note 1.

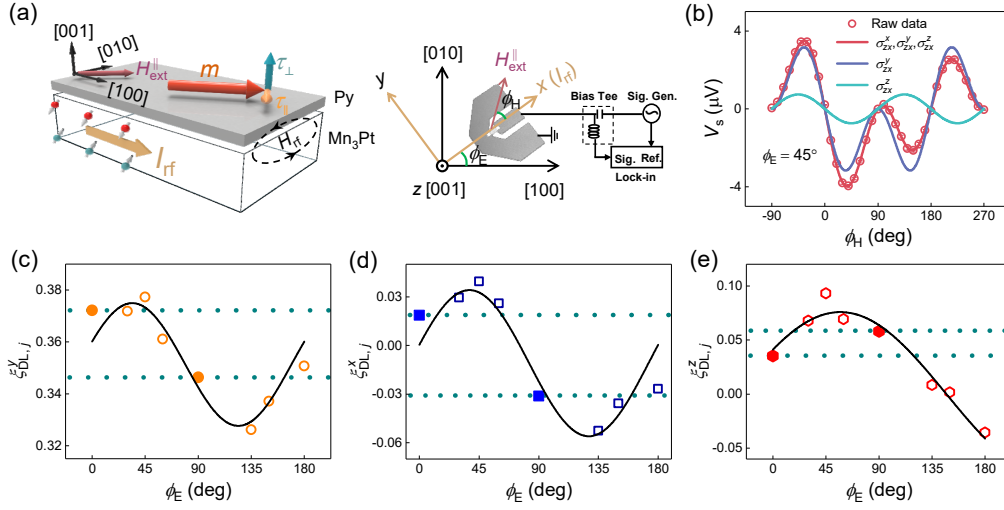


Fig. 2 Characterization of the SOT associated with σ_{ij}^p ($p = x, y, z$) by ST-FMR in Mn₃Pt/Py. **a**, (Left) The schematic of the Mn₃Pt/Py device. The magnetization m of the Py layer is set by an in-plane field and then subject to the in-plane SOT τ_{\parallel} and out-of-plane SOT τ_{\perp} associated with the spin current generated in Mn₃Pt. (Right) The schematic of the ST-FMR measurement setup. The electrical current I_{rf} is injected with an angle ϕ_E relative to the [100] direction of Mn₃Pt. For each device with a fixed ϕ_E , an in-plane external magnetic field $H_{\text{ext}}^{\parallel}$ is swept at an angle ϕ_H with respect to I_{rf} . **b**, Representative ϕ_H dependence of V_s at $\phi_E = 45^\circ$, where the symmetric component V_s is defined in Supplementary Note 3. The decomposition into contributions from the spin polarizations σ_{ij}^p can be derived from fittings (solid lines) to Eqs. (3). **c-e**, The ϕ_E dependence of the damping-like SOT efficiency per unit current density $\xi_{\text{DL},j}^p$ associated with σ_{ij}^p . The solid lines are fitting lines using Eq. (1). The anisotropy between $\phi_E = 0^\circ$ and $\phi_E = 90^\circ$ is highlighted by the enlarged symbols and dashed horizontal lines.

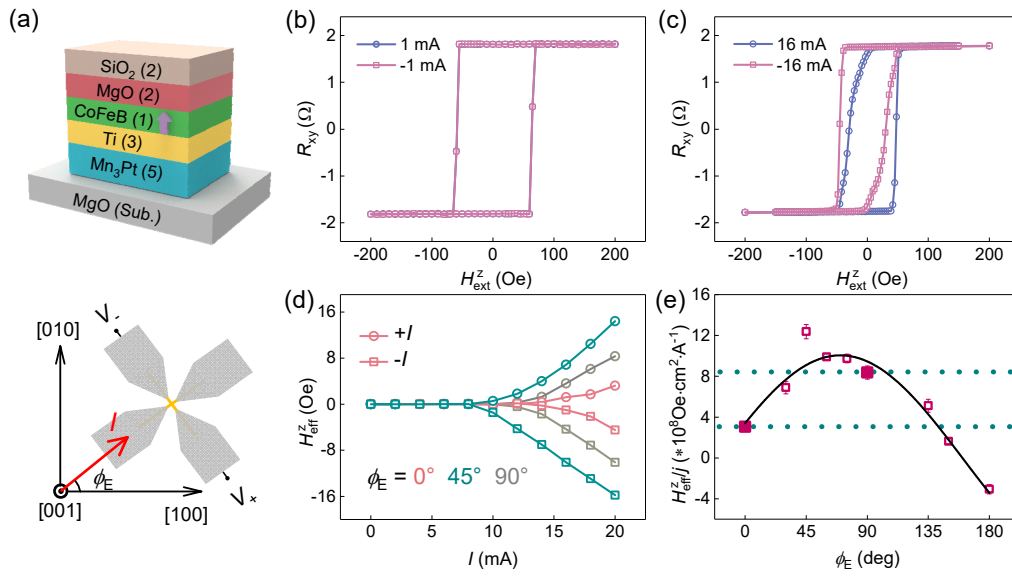


Fig. 3 AHE loop shift with a threshold current in Mn₃Pt/Ti/CoFeB/MgO/SiO₂. **a**, (Upper) The schematic of the Mn₃Pt/Ti/CoFeB/MgO/SiO₂ heterostructure, with numbers in parentheses indicate layer thickness in nanometers. (Lower) The schematic of the AHE loop shift measurement setup. **b**, The AHE loops under $I = \pm 1$ mA almost overlap with each other. **c**, Under $I = \pm 16$ mA, the AHE loops show an obvious shift towards positive or negative values. **d**, The I dependence of H_{eff}^z , which is defined as the shift of the AHE loop, at selected ϕ_E of 0° , 45° , and 90° . **e**, The ϕ_E dependence of the H_{eff}^z per unit current density. The anisotropy between $\phi_E = 0^\circ$ and $\phi_E = 90^\circ$ is highlighted by the enlarged symbols and dashed horizontal lines. The solid line is a fit to $\lambda_z \cos \phi_E + \mu_z \sin \phi_E$.

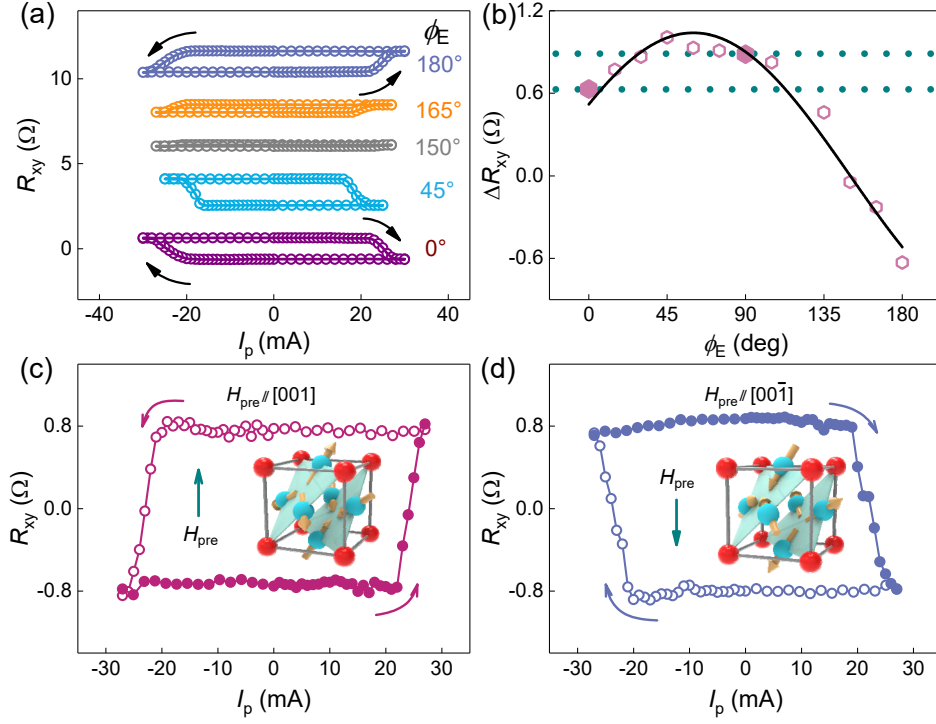


Fig. 4 Field-free deterministic magnetization switching and evidence for the MSHE in $\text{Mn}_3\text{Pt}/\text{Ti}/\text{CoFeB}/\text{MgO}/\text{SiO}_2$. **a**, The field-free deterministic switching of the CoFeB magnetization, represented by R_{xy} , for various ϕ_E . **b**, The ϕ_E dependence of the switching ratio, represented by ΔR_{xy} , which is the difference between R_{xy} at zero current after the application of the positive and negative current pulses. The anisotropy between $\phi_E = 0^\circ$ and $\phi_E = 90^\circ$ is highlighted by the enlarged symbols and dashed horizontal lines. The solid line is a fit to $\lambda_z \cos \phi_E + \mu_z \sin \phi_E$, suggesting again the combined effect of the conventional SHE and the MSHE. **c-d**, The switching polarity is reversed with premagnetization fields along opposite directions, a hallmark of the presence of the MSHE. The insets illustrate the spin configuration.

References

1. MacNeill, D. et al. Control of spin-orbit torques through crystal symmetry in WTe₂/ferromagnet bilayers. *Nat. Phys.* **13**, 300-305 (2016).
2. Song, P. et al. Coexistence of large conventional and planar spin Hall effect with long spin diffusion length in a low-symmetry semimetal at room temperature. *Nat. Mater.* **19**, 292-298 (2020).
3. Liu, L. et al. Symmetry-dependent field-free switching of perpendicular magnetization. *Nat. Nanotechnol.* **16**, 277-282 (2021).
4. Ikebuchi, T. et al. Crystal orientation dependence of spin Hall angle in epitaxial Pt/FeNi systems. *Appl. Phys. Lett.* **120**, 072406 (2022).
5. Chudnovsky, E. M. Intrinsic spin Hall effect in noncubic crystals. *Phys. Rev. B* **80**, 153105 (2009).
6. Freimuth, F., Blugel, S. & Mokrousov, Y. Anisotropic spin Hall effect from first principles. *Phys. Rev. Lett.* **105**, 246602 (2010).
7. Krén, E. et al. Magnetic structures and magnetic transformations in ordered Mn₃(Rh, Pt) alloys. *Phys. Lett.* **20**, 331-332 (1966).
8. Krén, E. et al. Magnetic structures and exchange interactions in the Mn-Pt system. *Phys. Rev.* **171**, 574 (1968).
9. Liu, L. et al. Current-induced switching of perpendicularly magnetized magnetic layers using spin torque from the spin Hall effect. *Phys. Rev. Lett.* **109**, 096602 (2012).
10. Liu, L. et al. Spin-Torque Switching with the Giant Spin Hall Effect of Tantalum. *Science* **336**, 555-558 (2012).
11. Zelezny, J., Zhang, Y., Felser, C. & Yan, B. Spin-Polarized Current in Noncollinear Antiferromagnets. *Phys. Rev. Lett.* **119**, 187204 (2017).
12. Hu, S. et al. Efficient perpendicular magnetization switching by a magnetic spin Hall effect in a noncollinear antiferromagnet. *Nat. Commun.* **13**, 4447 (2022).
13. Krén, E., Kádár, G., Pál, L. & Szabó, P. Investigation of the First - Order Magnetic Transformation in Mn₃Pt. *J. Appl. Phys.* **38**, 1265-1266 (1967).
14. Liu, Z. Q. et al. Electrical switching of the topological anomalous Hall effect in a non-collinear antiferromagnet above room temperature. *Nat. Electron.* **1**, 172-177 (2018).
15. Liu, L., Moriyama, T., Ralph, D. C. & Buhrman, R. A. Spin-torque ferromagnetic resonance induced by the spin Hall effect. *Phys. Rev. Lett.* **106**, 036601 (2011).
16. Garello, K. et al. Symmetry and magnitude of spin-orbit torques in ferromagnetic heterostructures. *Nat. Nanotechnol.* **8**, 587-593 (2013).
17. Sankey, J. C. et al. Measurement of the spin-transfer-torque vector in magnetic tunnel junctions. *Nat. Phys.* **4**, 67-71 (2008).
18. Nan, T. et al. Controlling spin current polarization through non-collinear antiferromagnetism. *Nat. Commun.* **11**, 4671 (2020).
19. Zhou, J. et al. Magnetic asymmetry induced anomalous spin-orbit torque in IrMn. *Phys. Rev. B* **101**, 184403 (2020).
20. You, Y. et al. Cluster magnetic octupole induced out-of-plane spin polarization

- in antiperovskite antiferromagnet. *Nat. Commun.* **12**, 6524 (2021).
21. Bai, H. et al. Control of spin-orbit torques through magnetic symmetry in differently oriented noncollinear antiferromagnetic Mn₃Pt. *Phys. Rev. B* **104**, 104401 (2021).
 22. Bose, A. et al. Tilted spin current generated by the collinear antiferromagnet ruthenium dioxide. *Nat. Electron.* **5**, 267-274 (2022).
 23. Bai, H. et al. Observation of Spin Splitting Torque in a Collinear Antiferromagnet RuO₂. *Phys. Rev. Lett.* **128**, 197202 (2022).
 24. Fang, D. et al. Spin-orbit-driven ferromagnetic resonance. *Nat. Nanotechnol.* **6**, 413-417 (2011).
 25. Thompson, R. et al. Anisotropic Spin-Orbit Torque through Crystal-Orientation Engineering in Epitaxial Pt. *Phys. Rev. Appl.* **15**, 014055 (2021).
 26. Baek, S. C. et al. Spin currents and spin-orbit torques in ferromagnetic trilayers. *Nat. Mater.* **17**, 509 (2018).
 27. Cao, C. et al. Efficient Tuning of the Spin-Orbit Torque via the Magnetic Phase Transition of FeRh. *ACS Nano* **16**, 12727 (2022).
 28. Pal, B. et al. Setting of the magnetic structure of chiral kagome antiferromagnets by a seeded spin-orbit torque. *Sci. Adv.* **8**, eabo5930 (2022).
 29. Kimata, M. et al. Magnetic and magnetic inverse spin Hall effects in a non-collinear antiferromagnet. *Nature* **565**, 627-630 (2019).
 30. Du, C., Wang, H., Yang, F. & Hammel, P. C. Systematic variation of spin-orbit coupling with *d*-orbital filling: Large inverse spin Hall effect in 3*d* transition metals. *Phys. Rev. B* **90**, 140407(R) (2014).